Accepted for presentation in: European Conference on Networks and Communications
& 6G Summit (EuCNC/6G Summit): Operational & Experimental Insights, June 2024.

Empowering 6G Industrial Indoor Networks: Hands-On Evaluation of IRS-enabled Multi-User mmWave Connectivity

Marco Danger, Simon Häger, Karsten Heimann, Stefan Böcker, and Christian Wietfeld
Communication Networks Institute (CNI), TU Dortmund University, 44227 Dortmund, Germany
E-mail: {Marco.Danger, Simon.Haeger, Karsten.Heimann, Stefan.Boecker, Christian.Wietfeld}@tu-dortmund.de

***Abstract*—The use of higher frequency bands beyond 6 GHz is considered to be key for future 6G networks. Yet, although generally available for licensing in an increasing number of countries, the 5G FR2 band has not seen much deployment for private networks so far in Europe. The main challenge for these higher frequency bands is proper beam management which allows to react flexibly to the radio conditions. This paper presents a systematic experimental evaluation of a commercial Millimeter-Wave (mmWave) indoor multi-user deployment in various reproducible channel conditions, in particular depending on Line-of-Sight (LOS) availability. We show that the beam management of the analyzed deployment can cope well with multi-user scenarios. When obstructing the LOS, alternative propagation paths are discovered and leveraged to avoid performance degradation. Only in extreme situations, such as in the case of an industry-typical safety cage that provides strong electromagnetic shielding, a significant performance decrease of the mmWave link is noted. To resolve such situations, we demonstrate that our passive Intelligent Reflecting Surface (IRS) solution HELIOS artificially introduces a qualitative reflection path that is seamlessly employed by the network to realize high-capacity communication in challenging radio environments utilizing a Beyond Line-of-Sight (BLOS) link. All-in-all, the evaluation demonstrates the promising potential of mmWave for real-life indoor factory deployments.**

***Index Terms*—mmWave communications, indoor measurements, beam management, multi-user, LOS/NLOS, reflecting surfaces.**

I. Introduction

5G introduces the use of the mmWave frequency spectrum, which offers a high amount of radio resources and thus enables scalable network capacities to meet growing wireless traffic demands. However, the utilization of this so-called Frequency Range 2 (FR2) of 5G New Radio (NR) is currently focusing on rather static and residential deployments, e.g., for Fixed Wireless Access (FWA) [1]. To realize the full capabilities of mmWave, the operation of FR2-enabled networks needs to be tested in challenging environments to validate their functionality, analyze their performance, and identify potential for improvement. Especially in industrial indoor environments, the dynamic surroundings, mostly in the form of metallic obstacles, as well as the high demands on performance and reliability are challenging tasks to be fulfilled by the mobile network. Due to the limitations caused by higher path losses at mmWaves, the combination with a so-called anchor cell in the conventional sub-6 GHz spectrum as well as the maintenance of LOS conditions is essential for reliable operations [2].

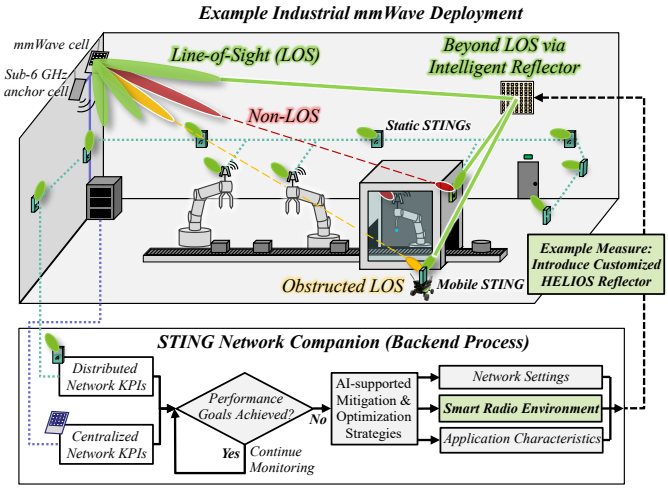

Fig. 1: Vision of 6G industrial networks in challenging environments: continuous monitoring and optimization of network KPIs using STING and HELIOS.

In Fig. 1, a demanding Indoor Factory (InF)-like environment is outlined in which several machines operate fully autonomously. To ensure reliable networking, they are connected to both mmWave (FR2) and sub-6 GHz (FR1) cells via Dual Connectivity (DC). The Spatially distributed Traffic and Interference Generation (STING) framework presented in [3] is used to gather performance data across the different frequency bands using multiple distributed mmWave-enabled STING devices. Furthermore, these key performance indicators (KPIs) are overlaid with centralized network KPIs within the so-called *STING Network Companion* to realize a comprehensive *KPI Monitoring and Control System*. Through continuous monitoring in the backend process, mitigation and optimization strategies are initiated when performance drops or potential improvements are identified. In future 6G networks, such central instance can serve as basis for an efficient Self-organizing Network (SON) [4].

In this paper, we deploy a private 5G network with multiple STING devices in a demanding industrial indoor scenario to evaluate the system performance, challenge its reliability, and present efficient mitigation strategies. After identifying the baseline performance with single-user measurements under LOS condition, the multi-user connectivity is assessed by placing the STINGs at different distances and angles relative to the cell. Obstacles are then introduced into the scenario to cre-

ate realistic Non-Line-of-Sight (NLOS) conditions, and thus, a more challenging radio environment. Finally, a mitigation strategy is presented by customizing the *Smart Radio Environment* in the form of our Holistic Enlightening of bLackspots with passIve reflectOr moduleS (HELIOS) concept [5]. This passive IRS creates BLOS conditions and thus improves the overall performance of the network, which emphasizes the promising potential of these reflectors for 6G. The results of our work verify the reliable operation of a mmWave network within a challenging industrial indoor environment. At the same time, the need for continuous performance monitoring is highlighted in order to initiate mitigation and optimization strategies, such as in the form of an IRS.

The remainder of this work is structured as follows. In Sec. II we discuss related work on experiments with mmWave networks and reflecting surfaces. Afterward, Sec. III describes the indoor scenario and STING-based KPI measurement methodology. We then evaluate the measurement results of our experiments in Sec. IV. At last, we summarize the results of this work in Sec. V and give an outlook on future works.

II. Potentials and Performance Assessments of mmWave Networks in Factory Environments

5G extended to mmWave frequencies primarily owing to the need for scalable network capacity and peak data rate improvements. These are achieved by utilizing the large contiguous bandwidth that is not available in the sub-6 GHz spectrum. However, this move is challenged by more hostile radio conditions due to higher propagation and obstacle penetration losses which are complemented by reduced diffraction. Although such effects are partially mitigated by the use of beamforming antenna arrays and novel beam management procedures, the cell radius of mmWaves is smaller than for sub-6 GHz frequencies. Additionally, mmWave networks suffer from a high likelihood of shadow regions within the cell's coverage where high data rates cannot be attained [6]. Against this background, they are well-suited for rather small-scale networks such as in InF scenarios where little infrastructure is needed for connectivity throughout the deployment scenario.

Globally, few public 5G mmWave networks have already been deployed providing peak Downlink (DL) data rates of up to about 2 Gbit/s to mmWave-capable smartphones [7, 8]. Yet the Uplink (UL) throughput was mostly disregarded. We note, however, that the authors in [9] emphasize the use of a DL-centric configuration which indicates much lower UL data rates. Moreover, it is further observed that the typical data rate is much lower depending on distance, antenna orientations, LOS/NLOS conditions, and user mobility [6, 9, 10]. The latter two options have been shown to cause handovers between cells and antenna beams, or even fallbacks to sub-6 GHz cells, cf. [7, 9, 10]. Furthermore, another dependency exists on the number of active users in the cell which is, for example, investigated in [7]. The mmWave connectivity is complemented by small Round-trip Times (RTTs) of typically about 15 ms and lower [6, 9, 11] with End-to-End (E2E) latencies over the internet being larger, e.g., 54 ms in [10].

The above-discussed works underline both the functioning and high potential of mmWave systems. However, the public nature of the networks under test only allows for a partial performance overview since there is limited knowledge about the network configuration in use and the measurements might be affected by other unaccounted users. In contrast, this work deliberately moves into an indoor scenario with a private 5G network allowing both access to network-internal states and a controllable amount of connected UEs. For this purpose, a mature 5G Non-Standalone (NSA) FR2 network infrastructure as well as off-the-shelf mobile devices are deployed, whereas in previous works such as [12] a rather experimental, software-defined radio based research platform was used for similar mmWave communication studies. Following the distributed performance evaluation blueprint for wireless networks proposed in [13], we study UL and DL KPIs provided by both the UEs and network infrastructure. Applying this approach to reproducible deployment scenarios using different network configurations, we conduct an in-depth performance evaluation of a modern mmWave network's Quality of Service (QoS).

In the context of current 6G research, IRSs are envisaged to illuminate such shadow regions, thus enabling BLOS connectivity [14]. After investigating the potential of IRS for vehicular mobile networks using simulations in [15], we proposed and evaluated our HELIOS concept [5] as a passive IRS. Passive IRSs such as HELIOS are custom-tailored solutions without power consumption that could be used in conjunction with current network generations as there is no need for a control link. Despite numerous practical insights into this field with experimental setups [16, 17], this work is – to the best of the authors' knowledge – the first to successfully demonstrate the use of a reflecting surface with a commercial cellular mmWave system in InF-typical conditions.

TABLE I: Configuration of 5G NSA / EN-DC mobile network.

	Parameter	Description/Value
Cell Configuration	**FR1 / LTE Anchor Cell**	
	Radio Unit	Ericsson Radio 2203
	Frequency Band	LTE band 7 (FDD)
	Center Frequency	2.65 and 2.53 GHz (DL/UL)
	Bandwidth	20 MHz
	Transmit Power	100 mW (EIRP)
	FR2 / NR mmWave Cell	
	Radio Unit	Ericsson AIR 1281
	Frequency Band	5G NR n257 (TDD)
	Frequency Range	26.7 to 27.5 GHz
	TDD Pattern	DDSU
	TDD Special Slot Pattern	11:3:0
	Component Carriers (CCs)	1, 4 or 8
	Bandwidth	100 MHz per CC
	Subcarrier Spacing (SCS)	120 kHz
	Transmit Power	100 mW (EIRP)
User Equipments	Number of Active Devices	up to three User Equipments (UEs)
	Device Model	Quectel 5GDM01EK with Quectel RG530F-EU
	Modem	Qualcomm SDX65
	mmWave Antenna Module	RA530T with four QTM547 (8×8, cross-polarized)
	LTE Category	Cat 20 / Cat 18 (DL/UL)
	5G NR Compliance	Release 16 NSA/SA
	Power Class	Class 3 (23 dBm)
	MIMO Capabilities	FR1: DL 4×4, UL 2×2 FR2: DL 2×2, UL 2×2

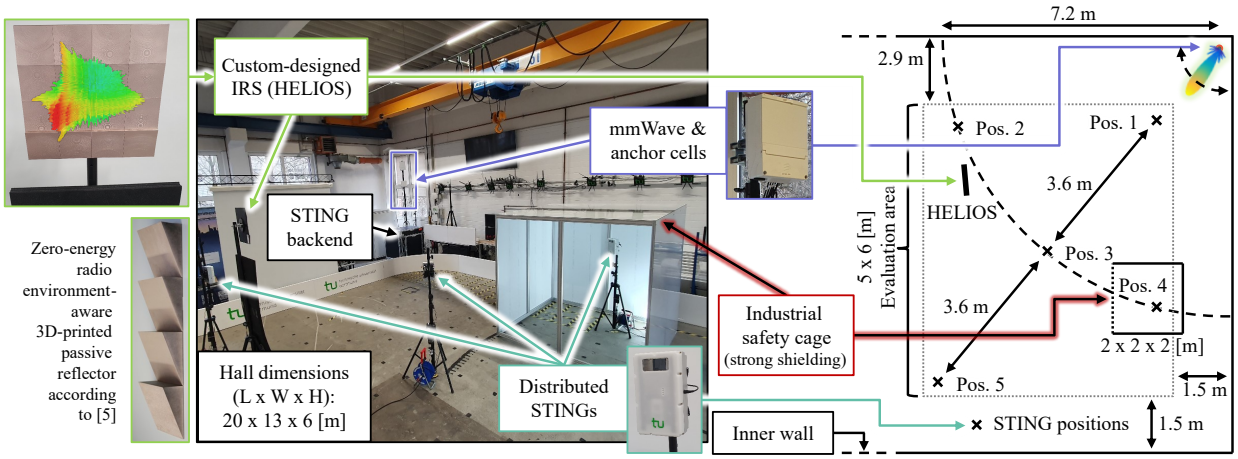

Fig. 2: Indoor environment for hands-on evaluation of IRS-enabled multi-user mmWave connectivity. *(Left)* Photo of setup with highlighted key components. *(Right)* Top view of lab environment introducing dimensions as well as STING, HELIOS, safety cage and cell positions.

III. Methodology for Distributed Performance Evaluation of Indoor mmWave Network

This section introduces the methodology of this manuscript. First, we introduce the architecture of our mmWave-enabled private 5G network in Sec. III-A. We subsequently present the deployment scenarios together with the measurement setups under test in Sec. III-B. Last, Sec. III-C describes our selection and acquisition of KPIs for the evaluation in Sec. IV.

A. mmWave Network Architecture

Tab. I summarizes the key configurations of the deployed 5G NSA mobile network operated in E-UTRAN / New Radio Dual Connectivity (EN-DC) mode. Both Long Term Evolution (LTE) anchor and NR mmWave cells are attached to a pole at the edge of the hall with a height of 3.0 m and 3.2 m, respectively. For our experiments, we enforce payload data transmissions via 5G NR FR2 by

- Utilizing only the Secondary Cell Group (SCG) bearer (i.e. no split bearer for simultaneous use of both links),
- Setting the minimum SINR for NR to −40 dB, and
- Disabling the Discontinuous Reception (DRX) mode (i.e. a form of NR power saving).

We employ up to three UEs as STINGs mounted on tripods at a height of 1.5 m, with the respective antenna arrays horizontally-aligned to the mmWave cell. By co-deploying each with a single-board computer that is remotely managed via an unimpaired control link, the *STING Network Companion* initializes payload transmissions for the KPI acquisition, see Sec. III-C.

B. Measurement Scenarios

On the left of Fig. 2, we show our indoor environment and highlight the various components that are used to create different measurement scenarios, particularly the STING modules and the radio units of the private network. Additionally, a safety cage, whose side walls can be removed in a modular fashion, and a HELIOS reflector as custom-designed passive IRS are used in some scenarios.

On the right side of Fig. 2, we sketch the indoor environment in top view. The gray boundary illustrates the $5\,\mathrm{m} \times 6\,\mathrm{m}$ evaluation area populated by the STINGs. Moreover, the five selected positions used to create three basic multi-user setups become apparent from this perspective:

1) *Co-Located*: All three STINGs are placed at position 3.
2) *Multi-Distance*: Three STINGs are distributed along Pos. 1, 3 and 5 enforcing different distances to the mmWave cell but at an identical azimuth angle.
3) *Multi-Angle*: Three STINGs are distributed along Pos. 2 to 4 that are equidistant to the mmWave cell but at different azimuth angles.

In addition to these placement strategies, Pos. 4 can be covered by the metallic safety cage to cater for a severe local obstruction and thus enforce an NLOS condition there. By opening the cage on one side, cf. depicted state on the left of Fig. 2, we attain an Obstructed Line-of-Sight (OLOS) link modality. Here, we subsequently introduce the passive IRS at a height of 2.2 m and horizontally align the STING antenna to the reflector. The employed Holistic Enlightening of bLackspots with passIve reflectOr moduleS (HELIOS) reflector [5] has an overall size of $40\,\mathrm{cm} \times 40\,\mathrm{cm}$ using a 4×4 module arrangement. The individual modules are curved with $c = 1\,\mathrm{m}$ imprinted sphere radius and have unique horizontal and vertical slopes (α, β) with up to 5.1° tilt angle. Electromagnetic simulations coupled with a differential evolution algorithm were employed to configure a broadened vertical reflection lobe with 17.8° beamwidth. The design was then 3D-printed and spray-coated with a conductive varnish, as shown on the left of Fig. 2 together with the reflection pattern in the form of the bistatic radar cross-section, simulated using *Ansys HFSS*. Subsequently, the latter is integrated into *Wireless InSite* ray-tracing yielding Radio Environmental Maps (REMs) along the evaluation area to compare and validate the measurement results. Within these simulations, a detailed digital twin of the indoor environment is used in addition to antenna and reflection characteristics in order to determine the radio propagation realistically. For this purpose, we combine individual subchannels from cell to IRS and from IRS to the UEs.

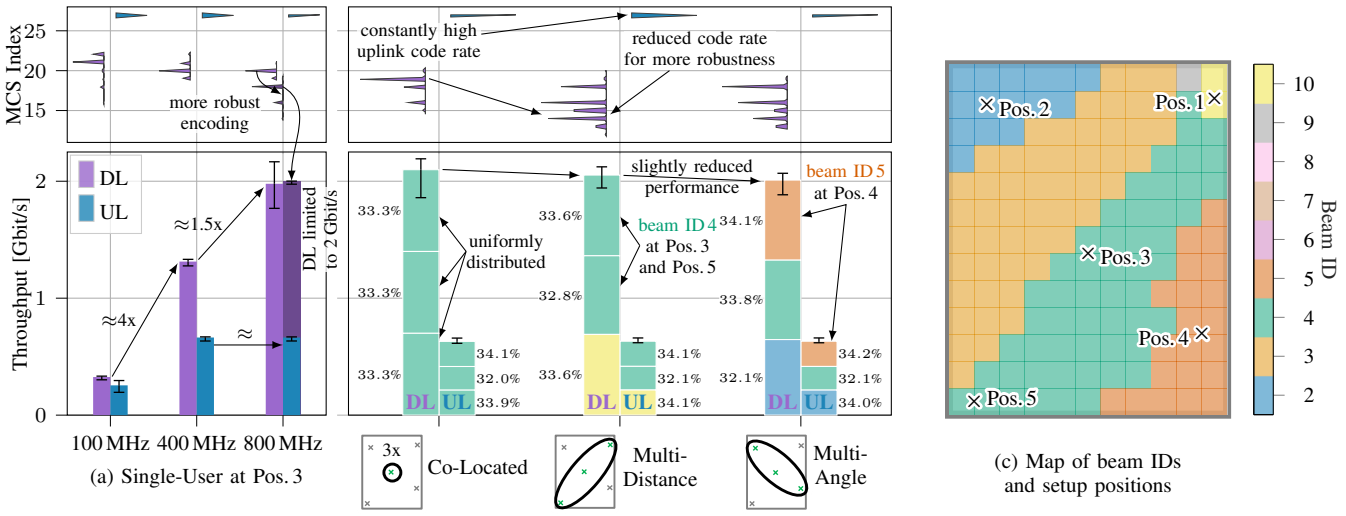

Fig. 3: Evaluation of LOS performance for single-user *(a)* and multi-user scenarios *(b)*, as well as measured beam IDs in evaluation area *(c)*.

C. Network and STING Performance Metrics

Employing the above-described measurement setups, KPIs are queried from both the mmWave cell and the STINGs as follows: We periodically retrieve baseband information from the mmWave cell. Each report accumulates usage values over a 1 s time period and includes the Physical Resource Block (PRB) utilization percentage (with 5 % resolution) and the Modulation and Coding Scheme (MCS) index (from 0 to 31) individually per Component Carrier (CC) as well as the Synchronization Signal Block (SSB) beam index (from 1 to 24). The beam indices correspond to a set of 24 wide beams arranged in a 6×4 grid in azimuth and elevation plane.

A specific *AT command* set is used to periodically request mmWave link information from the STING UEs by the co-deployed single-board computers. We query passive parameters, e.g., Reference Signal Received Power (RSRP) and Rank Indicator (RI), as well as active ones such as DL/UL MCS. Also, RTT and User Datagram Protocol (UDP) throughput measurements are conducted via *ping* and *iperf3*, respectively.

IV. Hands-on Evaluation of 5G mmWave Network

This section deals with the evaluation of the measurement scenarios from Sec. III-B. First, the end-to-end performance along different bandwidths is assessed using a single STING in Sec. IV-A. Then, the three different multi-user LOS setups are compared in Sec. IV-B regarding the overall network capacity and the per-user QoS. Sec. IV-C analyses the impact of deteriorating radio conditions due to a severe industry-typical obstacle. Finally, a passive IRS/HELIOS reflector is used as energy-efficient mitigation strategy for BLOS connectivity.

A. Single-user mmWave Connectivity in LOS

In this section we consider a STING at Pos. 3. Owing to the absence of competing UEs, this single network subscriber is expected to make use of the whole network capacity. The throughput is consecutively measured in UL and DL direction, while the number of active CCs in the cell is varied from one up to eight. This results in a bandwidth of the mmWave link of 100 MHz, 400 MHz and 800 MHz, respectively.

Fig. 3a shows the single-user measurement results. The view is split into the recorded distribution of the MCS index and the achieved application throughput. Measurements are conducted with a duration of 500 s for each configuration in terms of bandwidth and transmission direction. The STING is initially configured to aim for the maximum throughput. A maximum throughput of 669.8 Mbit/s and 2.2 Gbit/s for UL and DL is achieved, respectively. The latter matches the values reported in literature, cf. [7, 8]. The lower value in UL direction is explained as follows. On the one hand, the employed UE only supports up to 400 MHz transmission bandwidth, as we confirmed with a spectrum and signal analyzer during the experiments. On the other hand, as noted in Tab. I and [9], a DL-heavy Time Division Duplex (TDD) pattern causes an asymmetry, since the UL direction is scheduled only in 25 % of time. Besides, the DL data transmission at 800 MHz falls short of expectations, since with a doubled bandwidth (compared to 400 MHz) a nearly doubled throughput would be expected. Instead, the DL throughput only increases by a factor of 1.5 and is much more varying as indicated by the error bars. Without a complex investigation, it is not possible to determine the source of this variation, which can be in the mobile device, the network or the transport infrastructure troubled to carry the high traffic load. Anyhow, the end-to-end measurement framework seems to be limited. For this reason, we decided to restrict the STING application throughput to 2 Gbit/s at most, which leads to a less varying and on average higher DL throughput at a more robust MCS, as shown in dark purple.

The above throughput measurements exceed the ones attained in private sub-6 GHz 5G networks in which, e.g., an UL data rate of only 90 Mbit/s is achieved in [13], thus underlining the applicability for UL-heavy industry use cases. Additionally, we observe a mean RTT of 9.2 ms which is better

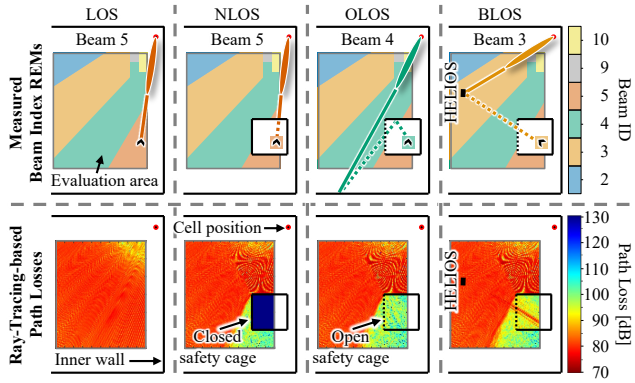

(a) Measured cell beam ID REMs complemented by ray-tracing-based path losses using all 24 beams along the evaluation area.

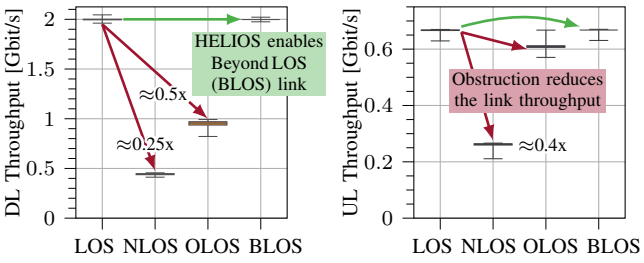

(b) Observed long-term throughput distributions for STING at Pos. 4.

Fig. 4: Resolution of NLOS situation by passive IRS HELIOS: Experimental results for different channel conditions ranging from LOS to Beyond Line-of-Sight (BLOS).

than reported for public networks in [6, 9] and the private Frequency Range 1 (FR1) deployment in [13].

The PRB utilization (not depicted for brevity) remains at a constantly high level of about 85 % to 90 %. However, it is noticeable in both link directions that not all radio resources are utilized. Restricting the application throughput to 2 Gbit/s slightly reduces the PRB utilization even though the mean throughput increases as discussed before.

The distribution of MCS indices shows that index 27 is used most of the time in UL direction. In DL, generally lower MCS indices are used most probably owing to the comparably lower transmission power and thus demand for a more robust encoding. With the restricted application throughput to 2 Gbit/s, the MCS even drops mostly to index 18 presumably due to the reduced traffic demand in favor of a more robust and thus stable link performance.

B. Scalability Analysis for Multi-user Setups

In this section, multi-user scenarios are analyzed in terms of MCS, throughput and beam management. As discussed in Sec. III-B, five monitoring positions, at different distances and angles from the cell, are considered. We first assess the implications of this on the beam management by recording the utilized SSB beam indices in 0.5 m steps within the evaluation area. Considering the resulting SSB beam ID REM in Fig. 3c, it shows the predominant use of beam indices 2 to 5. These beam configurations may facilitate the strongest main lobe downtilts. However, near the mmWave antenna (i.e., near Pos. 1) the STING is unexpectedly served by beams with higher elevation. Comparing the beam IDs observed during our three multi-user measurements to the above-discussed REM, we find that they match the prior REM record which thus underlines a stable assignment of serving beams.

Similar to the discussion of single-user measurements in Sec. IV-A, the multi-user measurement results in terms of both per-user and overall cell throughput are given in Fig. 3b. The stacked bars are colored according to the beam IDs at the respective mobile device positions. First, we observe in both directions a fair sharing of the overall throughput between the three devices among all scenarios. By placing the three STINGs in the same beam, the *co-located* setup attains the highest throughput. The *multi-distance* setup necessitates the use of beam ID 10 for the closest STING, while for the *multi-angle* setup, three different beam IDs are utilized for the STINGs. Coincidentally, a slightly reduced aggregated performance is observable along the separation to different beam IDs.

Looking at the distribution of MCS indices, a high code rate is constantly used in UL direction, while it varies for DL transmissions. The comparatively high index 19 is most frequently used within the *co-located* setup. In contrast, the more robust indices 13 to 18 are more frequently used for *multi-distance* and *multi-angle*, which corresponds to the reduced throughput. This strengthens our previous assumption that concurrent DL transmissions to UEs in different beams are less efficient than when using the same beam to *co-located* STINGs.

C. Operation in NLOS/OLOS Regimes with IRS

In this section, we move on to a challenging scenario in which the UE at Pos. 4 is fully obstructed by an industry-typical metallic cage (*NLOS*). We note that the SSB beam 5 remains in use, however, the RSRP is reduced by 33 dB. It is therefore significantly stronger than the 18 dB attenuation in the sub-6 GHz anchor, thus underlining the suitability of the Dual Connectivity (DC) concept. Studying the impact on the DL and UL throughputs in Fig. 4b, we observe drastic reductions from, on average, 1,995.9 Mbit/s down to 440.1 Mbit/s as well as 663.7 Mbit/s to 258.7 Mbit/s, respectively. This constitutes severe throughput reductions by 78 % and 61 % which thus affect the DL more than the UL, resulting from the transmission power control of the UE, that counteracts the created NLOS state.

Next, one side of the cage is removed to achieve *OLOS* connectivity by diffraction or multipath components which may find a way into the safety cage. On the one hand, this is confirmed by a cell-side switch to SSB beam 4, as sketched in Fig. 4a. On the other hand, we observe the NR RI changing from 1 to oscillating between 1 and 2, which is complemented by an, on average, 8 dB RSRP increase. Accordingly, the mean DL throughput increases to 949.4 Mbit/s, as shown in Fig. 4b, thus being approximately half the LOS but twice the NLOS throughput.

We now *install the passive IRS, in the form of the HELIOS reflector shown in Fig. 2, as mitigation strategy against this OLOS situation*. Following the ray-tracing-based prediction of

a strong reflection gain of about 25 dB towards Pos. 4, as shown in Fig. 4a, the SSB beam ID switches to 3 which matches the area in which the reflector is mounted. Compared to the prior reflector-less OLOS case, the NR RI is now stable at 2, thus underlining the quality of the attained path. Fig. 4b depicts the IRS-enabled mean DL throughput of 1,993.6 Mbit/s with little variance, thus constituting *BLOS connectivity* mitigating the impact of the obstruction entirely.

Lastly, we assess the UL throughput for the two OLOS cases. Whereas in NLOS the UL was severely affected, we find an average degradation of less than 55 Mbit/s in OLOS compared to LOS. Moreover, there is less variability in the throughput, which may be due to the higher receiver sensitivity on the mmWave cell side, as well as the aforementioned transmission power control of the UE, both of which compensate for the effects of obstructions on UL connectivity. Nonetheless, the passive HELIOS reflector seamlessly restores a stable maximum throughput as shown in Fig. 4, indicating a high feasibility of mmWave deployments for UL-dominant InF scenarios.

V. Conclusions and Outlook

In this work, we assessed the performance of a private cellular mmWave system in an indoor environment. We began our assessment with a single-user scenario leveraging different bandwidths. Whereas we attained a peak DL throughput above 2 Gbit/s using 800 MHz of bandwidth, more robust MCS were used such that a lower spectral efficiency was attained than with lower bandwidths. In the UL direction throughputs of up to 660 Mbit/s were attained depending on UE's bandwidth limitations and the TDD pattern. These high data rates were complemented by, on average, sub-10 ms RTTs. Based on this, we evaluated various multi-user scenarios in which the overall DL network capacity was the lowest if the UEs were served by different SSB beams, and the capacity is maximized the more the UEs are in the same beam at the same distance. The UL capacity was negligibly impaired. These results underline good scalability to future factory environments requiring UL-heavy connectivity in terms of data rate and capacity, as well as low latency.

We further studied the implications of NLOS and OLOS modalities, e.g., caused by an industry-typical safety cage around production devices, on short-range mmWave links. There, the DL throughput strongly deteriorated by up to 78 %, and the UL only severely in NLOS. As this affects the network capacity in multi-user networks, we introduced an IRS in the form of the passive HELIOS reflector to exhibit the desired reflection behavior. Thereafter, we observed that the network switches to another serving beam which corresponds to the area in which the reflector is installed. As a result, UL and DL traffic reached the same performance as in LOS. Thereby the compatibility of passive reflectors with current-generation network technology was showcased to optimize connectivity in challenging radio environments in a cost- and energy-efficient manner. Further, this highlights the promising possibilities of IRSs, which are envisioned for 6G.

In our future work, we will further challenge the mmWave system performance, particularly in terms of UE mobility. Furthermore, we will scale the experiments conducted to a larger industrial indoor environment in order to validate the results obtained. In parallel, we are investigating processes for scenario-specific IRS mounting positions and configurations.

Acknowledgment

This work has been funded by the German Federal Ministry of Education and Research (BMBF) in the course of the *6G-ANNA* project under grant no. 16KISK101 and the *6GEM Research Hub* under the grant no. 16KISK038 as well as by the Ministry of Economic Affairs, Industry, Climate Action, and Energy of the State of North Rhine-Westphalia (MWIKE NRW) along with the *Competence Center 5G.NRW* under grant no. 005-01903-0047.

References

[1] Ericsson. Mobility report 11/2023. [Online]. Available: www.ericsson.com/en/reports-and-papers/mobility-report

[2] L. Xie, S. Song, Y. C. Eldar, and K. B. Letaief, "Collaborative sensing in perceptive mobile networks: Opportunities and challenges," *IEEE Wirel. Commun.*, vol. 30, no. 1, 2023.

[3] C. Arendt, M. Patchou, S. Böcker, J. Tiemann, and C. Wietfeld, "Pushing the limits: Resilience testing for mission-critical machine-type communication," in *Proc. IEEE VTC-Fall*, Sep. 2021.

[4] A. Chaoub, A. Mämmelä, P. Martinez-Julia, R. Chaparadza, M. Elkotob, L. Ong, D. Krishnaswamy, A. Anttonen, and A. Dutta, "Hybrid self-organizing networks: Evolution, standardization trends, and a 6G architecture vision," *IEEE Commun. Stand. Mag.*, vol. 7, no. 1, 2023.

[5] S. Häger, K. Heimann, S. Böcker, and C. Wietfeld, "Holistic enlightening of blackspots with passive tailorable reflecting surfaces for efficient urban mmWave networks," *IEEE Access*, vol. 11, 2023.

[6] S. Mohebi, F. Michelinakis, A. Elmokashfi, O. Grondalen, K. Mahmood, and A. Zanella, "Sectors, beams and environmental impact on the performance of commercial 5G mmWave cells: An empirical study," *IEEE Access*, vol. 10, 2022.

[7] A. Narayanan, M. I. Rochman, A. Hassan, B. S. Firmansyah, V. Sathya, M. Ghosh, F. Qian, and Z.-L. Zhang, "A comparative measurement study of commercial 5G mmWave deployments," in *Proc. IEEE INFOCOM*, May 2022.

[8] P. Dinh, M. Ghoshal, D. Koutsonikolas, and J. Widmer, "Demystifying resource allocation policies in operational 5G mmWave networks," in *Proc. IEEE WoWMoM*, Jun. 2022.

[9] M. Ghoshal, Z. J. Kong, Q. Xu, Z. Lu, S. Aggarwal, I. Khan, Y. Li, Y. C. Hu, and D. Koutsonikolas, "An in-depth study of uplink performance of 5G mmWave networks," in *Proc. ACM SIGCOMM Wkshps.*, Aug. 2022.

[10] A. Narayanan, E. Ramadan, J. Carpenter, Q. Liu, Y. Liu, F. Qian, and Z.-L. Zhang, "A first look at commercial 5G performance on smartphones," in *Proc. ACM WWW*, Apr. 2020.

[11] J. Ansari, C. Andersson, P. de Bruin, J. Farkas, L. Grosjean, J. Sachs, J. Torsner, B. Varga, D. Harutyunyan, N. König, and R. H. Schmitt, "Performance of 5G trials for industrial automation," *MDPI Electronics*, vol. 11, no. 3, 2022.

[12] K. Heimann, J. Tiemann, D. Yolchyan, and C. Wietfeld, "Experimental 5G mmWave beam tracking testbed for evaluation of vehicular communications," in *Proc. IEEE 5GWF*, Sep. 2019.

[13] C. Arendt, S. Böcker, C. Bektas, and C. Wietfeld, "Better safe than sorry: Distributed testbed for performance evaluation of private networks," in *Proc. IEEE FNWF*, Oct. 2022.

[14] M. Di Renzo, M. Debbah, D.-T. Phan-Huy, A. Zappone, M.-S. Alouini, C. Yuen, V. Sciancalepore, G. C. Alexandropoulos, J. Hoydis, H. Gacanin, J. de Rosny, A. Bounceu, G. Lerosey, and M. Fink, "Smart radio environments empowered by reconfigurable AI meta-surfaces: An idea whose time has come," *EURASIP J. Wirel. Commun. Netw.*, vol. 1, no. 129, 2019.

[15] K. Heimann, B. Sliwa, M. Patchou, and C. Wietfeld, "Modeling and simulation of reconfigurable intelligent surfaces for hybrid aerial and ground-based vehicular communications," in *Proc. ACM MSWiM*, Nov. 2021.

[16] J.-B. Gros, V. Popov, M. A. Odit, V. Lenets, and G. Lerosey, "A reconfigurable intelligent surface at mmWave based on a binary phase tunable metasurface," *IEEE Open J. Commun. Soc.*, vol. 2, 2021.

[17] R. Liu, J. Dou, P. Li, J. Wu, and Y. Cui, "Simulation and field trial results of reconfigurable intelligent surfaces in 5G networks," *IEEE Access*, vol. 10, 2022.